Lifetime analysis of ^{128,130}Te via the Doppler-shift attenuation method

Sarah Prill[1],* Anna Bohn[1], Vera Everwyn[1], Guillaume Häfner[1,2], Felix Heim[1], Mark Spieker[3], Michael Weinert[1], Julius Wilhelmy[1], and Andreas Zilges[1]
[1] *University of Cologne, Institute for Nuclear Physics, 50937 Köln, Germany*
[2] *Université Paris-Saclay, CNRS/IN2P3, IJCLab, F-91405 Orsay, France and*
[3] *Florida State University, Department of Physics, Tallahassee, Florida 32306, USA*
(Dated: January 11, 2022)

Background: The Z=52 nuclei ^{128}Te and ^{130}Te are interesting candidates to study nuclear-structure properties close to the Z=50 shell. The knowledge of lifetimes of low-lying states in those nuclei is still scarce.

Purpose: The goal of the present work is to extend the experimental database of nuclear level lifetimes of low-spin states in ^{128}Te and ^{130}Te.

Methods: Nuclear level lifetimes were determined by means of the Doppler-shift attenuation method (DSAM) using p-γ coincidences measured at the SONIC@HORUS setup located at the FN-Tandem ion accelerator of the University of Cologne.

Results: For ^{128}Te, lifetimes of eleven excited states could be determined, one of these for the first time. For the case of ^{130}Te, 18 nuclear level lifetimes were obtained, 15 for the first time. In both experiments, upper limits for lifetimes of several additional levels were determined. Moreover, the nuclear level scheme of ^{130}Te could be extended. One additional level and 13 new transitions for levels above 2.7 MeV have been added. A standard shell-model calculation was performed and compared to the experimental results, showing an overall agreement.

Conclusion: DSAM using pγ coincidences is a powerful tool to determine lifetimes in the sub-picosecond range free of feeding contributions. Although both experiments yielded low statistics, numerous lifetimes could be obtained. The use of pγ coincidences furthermore enables the extension of level schemes.

I. INTRODUCTION

With only two protons above the Z=50 nuclear shell closure, the tellurium isotopic chain is a valuable candidate for the systematic study of nuclear properties. In addition, the heaviest stable Te isotopes come close to the neutron shell closure at N=82. Information about low-spin states of heavy stable Te isotopes is still scarce [1–4], especially concerning lifetimes and absolute transition strengths of excited states.

Level lifetimes are fundamental properties of atomic nuclei and give direct access to nuclear structure properties. In combination with spin and parity quantum numbers of the involved states, the multipolarity, and the γ-decay branching ratio of a given γ-ray transition, the nuclear level lifetime of the initial state can be used to determine absolute transition probabilities.These transition probabilities are a stringent test for nuclear models and help to judge their predictive power.

In this way, nuclear transition probabilities also help to identify collective features of atomic nuclei such as mixed-symmetry states (MSS) in even-even nuclei. Here, a strong $M1$ decay to the 2_1^+ state and a weakly collective $E2$ transition to the ground state are expected for the lowest MSS [5]. Mixed-symmetry states in the stable even tellurium isotopes were already studied by Hicks *et al.* [1], observing a fragmentation of the transition strength.

Excited nuclear states can have lifetimes varying over a wide range from 10^{-18} s for the fastest $E1$ decays to 10^{15} s for some isomeric states. Different methods are required to scan the whole range [6]. The lifetimes relevant in our case are in the order of picoseconds and below. The determination of those lifetimes is achieved with the Doppler-shift attenuation method (DSAM)[7–11].

Some of the former measurements of short-lived level lifetimes in the tellurium isotopes have been performed by inelastic neutron scattering (INS) [1, 2, 12, 13]. However, the scattered projectile is not detected in such INS-DSAM experiments. Unknown feeding of the states of interest from higher-lying states can lead to wrong lifetime assignments. This can only be avoided by performing experiments with many different beam energies. As a result, typically only so-called "effective" lifetimes are measured.

In this paper, lifetimes of short-lived excited low-spin states in ^{128}Te and ^{130}Te have been measured with the pγ-coincidence DSA technique that uses the coincident information of excitation and decay to precisely determine level lifetimes by selecting the excitation of interest. Thus, feeding from higher-lying levels can be eliminated. In Sec. II, the experimental details of both experiments are provided, followed by a description of the pγ-coincidence Doppler-shift attenuation (DSA) technique in Sec. III. The results are discussed in Sec. IV and summarized in Sec. V.

II. EXPERIMENTAL DETAILS

Lifetimes of excited nuclear low-spin states in ^{128}Te and ^{130}Te have been studied using particle-γ coincidence spectroscopy in two inelastic proton-scattering ex-

* prill@ikp.uni-koeln.de

periments. Both experiments were performed at the 10 MV FN-Tandem accelerator of the Institute of Nuclear Physics at the University of Cologne. Proton-beam energies of 8.8 MeV and 10 MeV were used for the scattering experiments on ^{128}Te and ^{130}Te, respectively.

Particle-γ coincidence data have been collected at the SONIC@HORUS detector array [14]. The particle-identification chamber SONIC serves as a particle detector array as well as a target chamber. It contains 12 passivated implanted planar silicon (PIPS) detectors mounted in three rings at backward angles, providing a solid-angle coverage of 9%. SONIC is surrounded by the γ-ray detector array HORUS. It consists of 14 High Purity Germanium (HPGe) detectors positioned at five different angles with respect to the beam axis. Six detectors are equipped with active BGO Anti-Compton shields. Further details of SONIC@HORUS are given in Refs. [14–16]. Next to the target, a ^{56}Co source was mounted and its decays were continuously measured to allow the precise energy calibration as well as energy-shift tracking. The recorded data from the (p,p'γ) experiments have been sorted by setting a trigger condition on the detected protons. To assign each detected proton to the respective excitation energy E_x of the target nucleus, the particle spectra were calibrated by setting a gate on known γ-ray decays of the target nucleus. The energies of the coincident protons were then converted into corresponding excitation energies. In total, the (p,p'γ) experiments on ^{128}Te and ^{130}Te yielded enough statistics to analyze nuclear levels robustly up to excitation energies of E_x=3.0 MeV and E_x=3.6 MeV, respectively.

A. Target properties

Both targets consisted of a thin layer of Te target material deposited on a natural Ta backing to ensure the complete stopping of the recoiling nuclei which is necessary for lifetime determination with the Doppler-shift attenuation method (DSAM). The isotopic enrichment was 99.5(1)% for ^{128}Te and 99.3(1)% for the ^{130}Te target, respectively. The targets were produced by rolling the Ta stopper to the desired thickness and consecutively evaporating the target material on top. The layers were weighed after each step, giving an average areal density of 0.4(1) mg/cm^2 for ^{128}Te and 0.5(1) mg/cm^2 for ^{130}Te, as well as 1.0(1) mg/cm^2 for the Ta stoppers. As weighing yields only average values, these areal densities can be different at the beam spot. For the determination of lifetimes with DSAM, however, precise knowledge of the target composition and areal density is necessary.

Therefore, a Rutherford backscattering (RBS) [17] experiment was performed at the RUBION facility in Bochum. With an alpha beam of 3 MeV RBS spectra were recorded at the position of the beam spot as well as 3 mm above and 4 mm below for each target to estimate the variation throughout the target. For complete beam stopping, a thick silicon layer was placed behind the target. Comparison of the spectra for different positions on the target shows an increase in thickness along the stopper layer due to the rolling as well as a higher density in target material towards the center as expected from evaporating material onto the stopping layer. For further analysis, the areal density at the beam spot is used, with the variation towards the edges considered in the uncertainty. The variation of thickness in the stopper layer can be neglected since all measured areal densities guarantee a full stopping of the recoil nuclei.

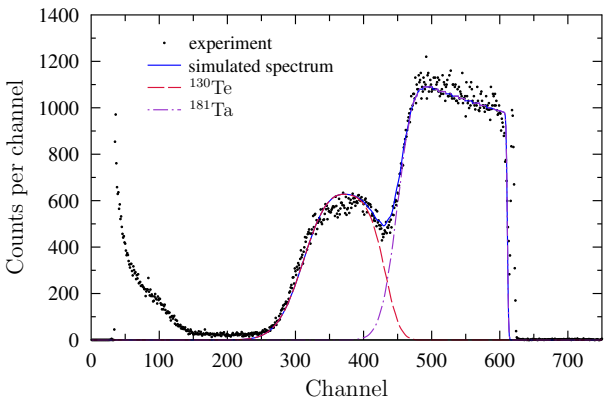

FIG. 1. Experimental (black dots) and simulated (blue solid line) RBS spectrum for the ^{130}Te target and its ^{181}Ta backing. The contribution of the target layer is given in red dashed, that of the backing in purple point-dashed. The backing was positioned in the direction of the RBS beam. The narrow peak of a pulser of known energy is visible to the right of the simulated spectrum.

The experimental spectrum for the beam-spot measurement for ^{130}Te as well as spectra simulated using SIMNRA [18] are given in Fig. 1.

For the ^{130}Te target, the areal density of ^{130}Te amounted to 0.58(5) mg/cm^2 and the areal density of the tantalum stopper to 1.15(9) mg/cm^2. For ^{128}Te, the RBS spectrum revealed oxygen contributions in the target layer. No such increased amount of oxygen in the target could be observed in the ^{128}Te(p,p'γ) spectra. We assume that an oxide formed after the DSAM measurement because the RBS measurement has been performed more than one year after the DSAM experiment.Therefore we use the weighed areal densities for the case of ^{128}Te in the following analysis.

III. DATA ANALYSIS

The Doppler-shift attenuation method (DSAM) is based on the idea that a γ-ray is emitted while the de-exciting nucleus is still in motion. The Doppler-shifted energy E_γ depends on the angle Θ under which the emitted γ-ray is observed with respect to the direction of the recoiling nucleus as well as on the velocity v of the nucleus at the time of de-excitation. Since the motion of the

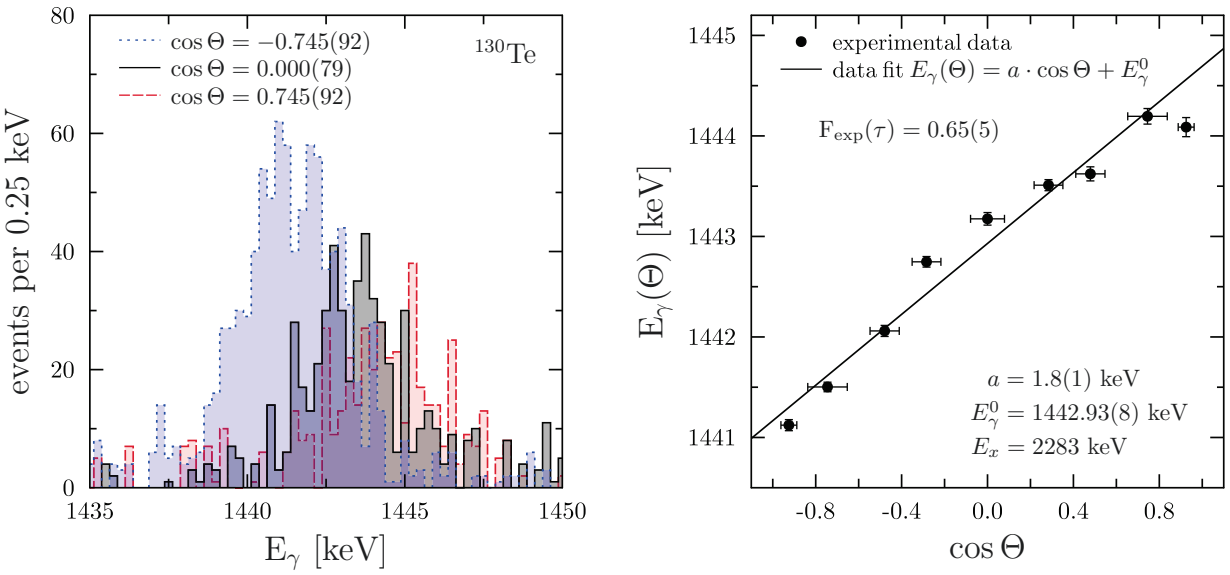

FIG. 2. Left: Region of the excitation-energy gated γ-ray spectrum around the energy of the strongest transition with $E_\gamma^0 = 1443$ keV of the ^{130}Te level at $E_x = 2283$ keV for three angular groups. Right: Linear fit to the energy centroids of the Doppler-shifted γ-decays determined from nine different angular groups for the same transition of the level at 2283 keV.

nucleus through the target material starts directly after its excitation with a velocity v_0 and its velocity continuously decreases along its path, the mean lifetime of the excited state can be extracted from the analysis of the Doppler shifts. For recoil velocities of $v_0 \approx 0.2$ % c, as observed in both experiments, the Doppler shift of the γ-energy is given by

$$E_\gamma(\Theta, \tau, v_0) = E_\gamma^0 \left(1 + \frac{v_0}{c} F(\tau) \cos\Theta\right) \qquad (1)$$

where E_γ^0 is the unshifted γ-ray energy. $F(\tau)$ is the so-called Doppler-shift attenuation factor which connects the observed Doppler shift to the lifetime of the excited state.

The combined SONIC@HORUS setup provides complete reaction kinematics from detecting the scattered particle in coincidence with the emitted γ-ray. The energies and positions registered with the 168 particle and γ-ray detector combinations thus yield the angle Θ as well as v_0 and E_γ^0. To extract $F(\tau)$ and finally τ from the data, all detector combinations are sorted into groups according to their corresponding Θ. The number of angular groups results as a compromise between sufficient statistics in each group by adding detector combinations of similar Θ, thus increasing the uncertainty in Θ, and the need for a well defined Θ. Depending on the intensity of the analyzed transitions, five to nine angular groups were chosen individually for the levels studied in both experiments. Due to energy and momentum conservation Θ also depends on E_x. Thus, the detector combinations sorted into the angular groups can change between different levels.

An excitation-energy gate on the level of interest is then applied to the p-γ matrices of each angular group, thus excluding feeding contributions from higher-energetic excitations [11]. Fitting the energy centroid of the coincident transitions in each group then yields the linear dependence of E_γ as a function of $\cos\Theta$ which results in $F(\tau)$, c.f. Eq. (1). In Fig. 2, this is illustrated exemplarily for the $E_\gamma = 1443$ keV transition of the tentative 2^+ state at $E_x = 2283$ keV. In the left panel, the excitation-energy gated spectrum around the transition energy is plotted for three different angular groups. No shift is observed in the spectrum with detector combinations belonging to $\Theta \approx 90°$ (solid grey spectrum). At forward angles, a shift towards higher energies is observed (red dashed spectrum), and for backward angles a shift towards lower energies can be measured (blue dotted spectrum). Extracting the energy-centroid of the peak in each angular group then yields the linear dependence shown in the right panel of Fig. 2. From the linear fit to the energy centroids the experimental attenuation factor $F_{exp}(\tau)$ is calculated.

A. Stopping process simulation

A Monte-Carlo simulation of the stopping process of the recoil nucleus in the target material has been performed to extract the lifetime from $F(\tau)$, connecting the measured attenuation to the corresponding time.

For this purpose, the stopping power as described in the stopping theory by Lindhard, Scharff and Schiøtt (LSS) [19, 20] is used, with the dimensionless variables ϵ

and ρ for the energy of the recoil nucleus and the distance it travelled through the stopping material, respectively,

$$\frac{d\varepsilon}{d\rho} = \left(\frac{d\varepsilon}{d\rho}\right)_e + f_n \left(\frac{d\varepsilon}{d\rho}\right)_n \quad . \tag{2}$$

The nuclear component (index n) describes discrete energy losses due to collisions with nuclei in the surrounding material via a Thomas-Fermi potential, modulated by an empirical reduction factor of $f_n = 0.7$ to account for deviations from this potential [11, 21–23]. The continuous stopping caused by surrounding electrons is reflected in the electronic stopping power. It is obtained by a fit to the semi-empirical stopping-power tables by Northcliffe and Schilling (NS) [24], with a correction for the atomic structure of the stopping medium as presented by Ziegler and Biersack [25, 26].

The Monte-Carlo simulation of the stopping process is performed with the code DSTOP96_PPPRIME_2, a modification of the DESASTOP code by Winter [27, 28]. It yields a dependence of the attenuation factor on the lifetime for a certain excitation energy of a nucleus stopped in the target and backing material under the given experimental conditions. This is denoted as theoretical attenuation factor $F_{theo}(\tau)$ in the following. The dependence is plotted in Fig. 3 for the 2^+ state of ^{130}Te at $E_x = 2283$ keV. The lifetime is then obtained by projecting the experimentally determined attenuation factor $F_{exp}(\tau)$ onto the x-axis, as indicated in Fig. 3. The statistical uncertainty $\Delta\tau_{stat}$ is determined by projecting maximal and minimal values of $F_{exp}(\tau)$ within its uncertainty interval. Since $F_{theo}(\tau)$ does not linearly depend on the lifetime, the resulting uncertainty interval of the lifetime is asymmetric with larger uncertainties towards higher lifetimes. Due to the decreased slope towards both ends of the curve lifetimes can only be extracted with large uncertainties in these ranges, limiting the lifetimes that can be measured with the given setup and configuration to few femtoseconds up to 1 ps.

The uncertainty of the calculation of the stopping process is determined by variation of the input parameters within their uncertainty interval and projecting $F_{exp}(\tau)$ onto the attenuation factor curve simulated with these. Those input parameters are the nuclear and electronic reduction factors as well as the areal density. As indicated for the state at $E_x = 2283$ keV in ^{130}Te in Fig. 4, the areal density has only a small impact on the measured values in the range of a few femtoseconds. For a precise stopping simulation, a good understanding of the composition of the targets is nonetheless necessary, as was shown in Ref. [29]. The nuclear reduction factor f_n is usually assumed to have no uncertainty but as it is determined empirically an uncertainty of 10% was assumed, as in Ref. [11]. This results in the largest contribution to the uncertainty of the attenuation factor dependence. The variation of f_e by 10% takes uncertainties in the knowledge of the stopping power into account [11]. The systematic uncertainty $\Delta\tau_{sys}$ of the lifetime is calculated as the geometric mean of these uncertainties.

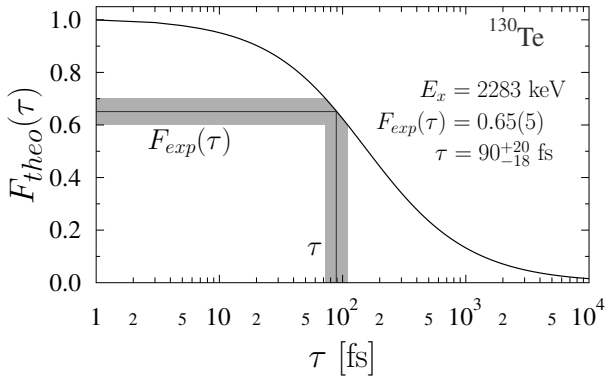

FIG. 3. Simulated dependence of the attenuation factor $F_{theo}(\tau)$ on the lifetime τ for the 2^+ level at $E_x = 2283$ keV of ^{130}Te and the attenuation factor $F_{exp}(\tau)$ derived from experiment. The determination of τ by projection of the experimentally obtained $F_{exp}(\tau)$ and its statistical uncertainty, indicated by the grey bars, are shown.

In the final representation of the lifetime two sets of asymmetrical uncertainties are given as $\tau \pm \Delta\tau_{stat} \pm \Delta\tau_{sys}$. We note that the overall uncertainties result from a very cautious error analysis.

IV. RESULTS AND DISCUSSION

A. Level lifetimes in ^{128}Te

In a beam time of four days experimental attenuation factors for eleven excited states in ^{128}Te could be extracted. The corresponding shifts are shown in Fig. 5. For states where the lifetime was too long to observe an unambiguous shift in the spectra, lower limits of about a few picoseconds could be assigned. This was possible for the levels at excitation energies 2028 keV, 2133 keV, 2517 keV, 2655 keV and 2932 keV.

The simulation of the stopping process of the recoiling nucleus was performed with the weighed areal densities as input parameters for the target properties, with the electronic stopping powers obtained as described in Sec. III A. The results from the Monte-Carlo calculation were compared to the experimental attenuation factor, yielding the lifetimes τ given for all eleven states in Tab. I. The lifetime of the 4^+ level at 1497 keV was determined for the first time, although with a large uncertainty due to the low statistics in combination with the small transition energy.

All lifetimes determined for ^{128}Te are illustrated in the level scheme on the left side of Fig. 6 as blue bars. The level scheme includes all levels for which lifetimes were accessible with DSAM and the transitions that were used for this analysis, as well as important low-lying levels

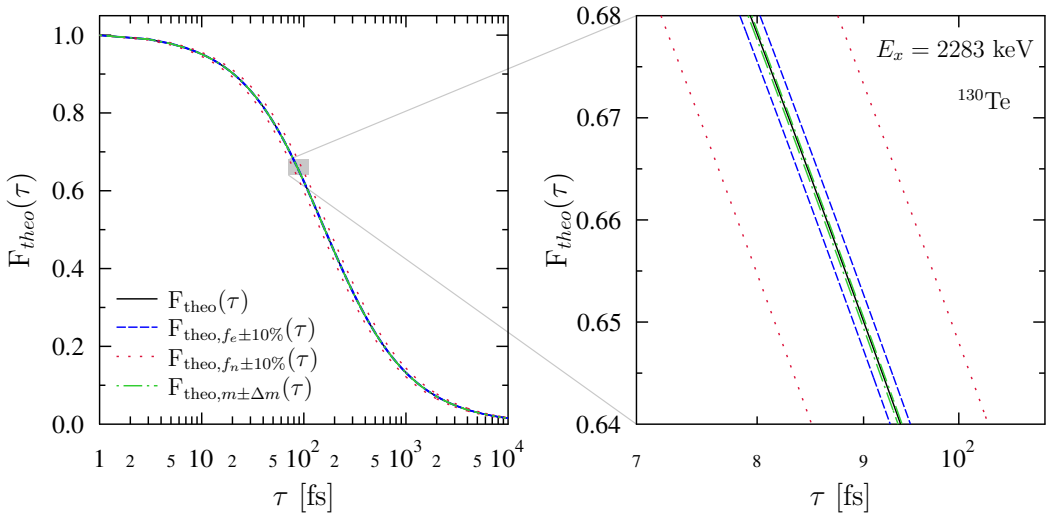

FIG. 4. Theoretical dependence $F_{theo}(\tau)$ on the lifetime simulated for the maximal deviations of the uncertainty of different input parameters for the 2^+ state of ^{130}Te at $E_x = 2283$ keV. The electronic (f_e, dashed) and nuclear reduction factor (f_n, dotted) are varied by 10%, whereas the areal density (m, dashed-dotted) is varied within its determined uncertainty.

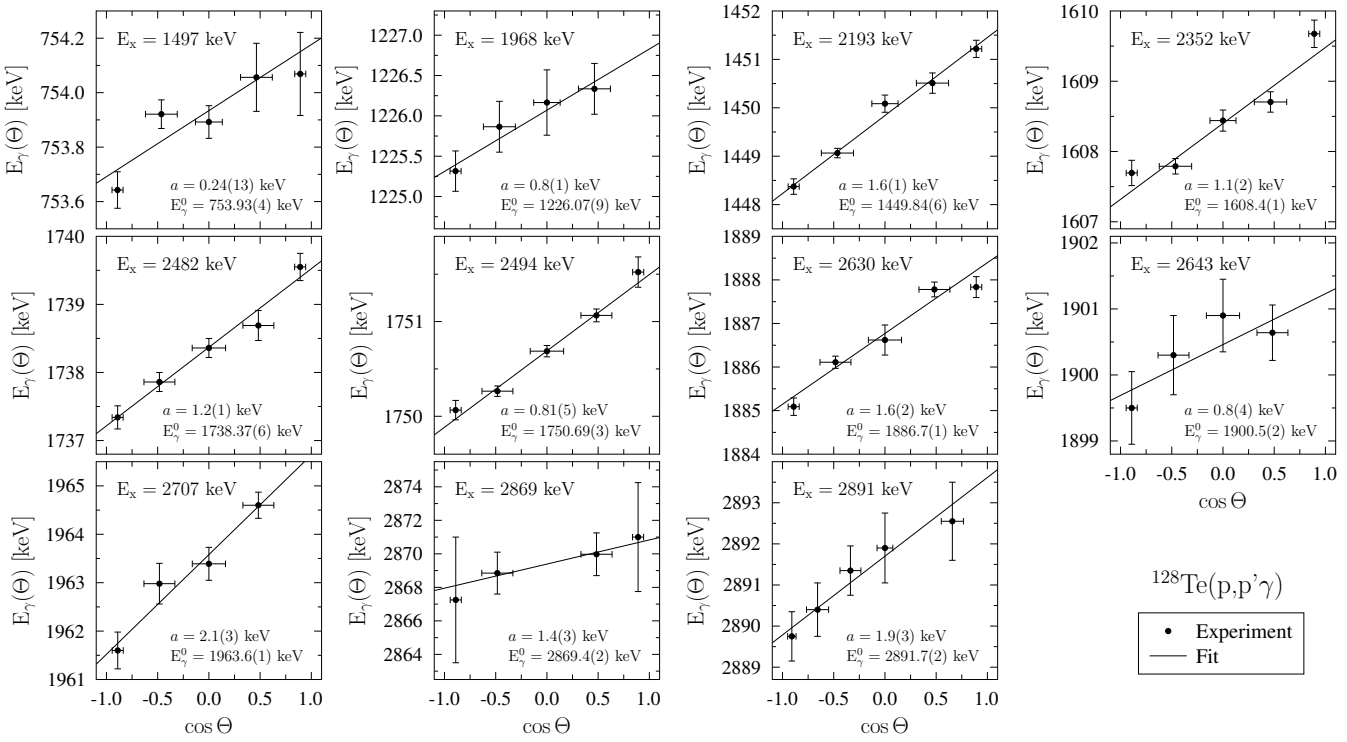

FIG. 5. Linear fits to the energy centroids of the Doppler-shifted γ-decays for all transitions in ^{128}Te from which lifetimes could be extracted. The number of angular groups varies according to the statistics for each transition. The slope a and unshifted transition energy E^0_γ are given in each case.

and their decays. As low statistics limit the analysis to levels that shift strongly, the majority of the analyzable levels have comparably short lifetimes, as visible in the illustration.

Along with the calculated level lifetimes for ^{128}Te, existing values reported by Hicks *et al.* [2] are given in Tab. I. The latter ones originate from an inelastic neutron scattering DSAM (INS-DSAM) experiment performed at the University of Kentucky and were measured without neutron-γ coincidences [2]. As one can see from Tab. I, the values from Ref. [2] are in very good agreement with the present work. The overall statistics of

TABLE I. Lifetimes of levels in ^{128}Te. Experimental attenuation factors $F_{exp}(\tau)$ and lifetimes τ are given. Statistical and systematic uncertainties for the lifetimes, $\Delta\tau_{stat}$ and $\Delta\tau_{sys}$, respectively, are stated as $\tau \pm \Delta\tau_{stat} \pm \Delta\tau_{sys}$. For the attenuation factors, only statistical uncertainties are given. Excitation energies E_x, transition energies E_γ and level spins and parities for the level of interest J_i^π as well as the final level J_f^π are taken from [3] if not stated otherwise. τ_{lit} are taken from [2]. From mixing ratios given in [3] and the lifetimes τ, $B(E2)\downarrow$ and $B(M1)$ transition strengths were calculated. Due to the asymmetric uncertainties of the lifetimes, Gaussian error propagation is not possible. Instead, the boundary values of the lifetimes were used to calculate intervals for the transition strengths, with the width of these intervals given in the way as upper and lower uncertainties are shown. The intervals were calculated for $\Delta\tau_{stat}$ and $\Delta\tau_{sys}$ individually and added quadratically in the respective direction.

E_x [keV]	J_i^π	E_γ [keV]	J_f^π	$F_{exp}(\tau)$	τ [fs]	τ_{lit} [fs]	$B(E2)\downarrow$ [e^{2}fm^4] [a]	$B(M1)$ [μ_N^2][a]
1497	4^+	753	2^+	0.17(9)	$741^{+1072\ +172}_{-280\ -124}$		4524^{+2901}_{-2807}	
1968	1^+,2^+,3^+	1225	2^+	0.35(10)	$284^{+166\ +68}_{-93\ -46}$	301^{+25}_{-22}	44^{+23}_{-18}	0.10^{+5}_{-4}
2193	2^+	1450	2^+	0.61(6)	$104^{+28\ +25}_{-24\ -17}$	72(2)	15^{+5}_{-4}	0.16^{+6}_{-5}
2352	2^+	1609	2^+	0.37(7)	$257^{+90\ +61}_{-62\ -43}$	198^{+14}_{-10}	13^{+5}_{-4}	0.043^{+16}_{-14}
2482	0^+[b]	1739	2^+	0.36(5)	$273^{+63\ +65}_{-48\ -44}$	290^{+80}_{-50}	188^{+54}_{-50}	
2494	$(3)^-$	1751	2^+	0.26(2)	$420^{+43\ +100}_{-37\ -68}$	340^{+40}_{-30}		
2630	3^+[b]	1887	2^+	0.48(8)	$167^{+58\ +40}_{-43\ -27}$	137^{+15}_{-14}	148^{+60}_{-49}	0.010^{+4}_{-3}
2643	?	1900	2^+	0.23(13)	$481^{+854\ +116}_{-225\ -78}$	230^{+78}_{-120}	69^{+62}_{-46}	
2707	1^+,2^+,3^+	1963	2^+	0.63(14)	$93^{+67\ +23}_{-44\ -15}$	115(8)	150^{+138}_{-70}	0.020^{+19}_{-10}
2869	(1),2^+[b]	2869	0^+	0.30(12)	$347^{+349\ +85}_{-141\ -56}$	410^{+180}_{-99}	5^{+4}_{-3}	
2891	2^+	2891	0^+	0.38(8)	$244^{+112\ +58}_{-70\ -40}$	270^{+42}_{-34}	12(5)	

[a] Intervals are given instead of uncertainties. See caption.
[b] J_i^π taken from [2].

the ^{128}Te(p,p'γ) reaction for many of the analyzed levels forced the use of fewer DSAM angular groups. In combination with an uncertainty of 10 % assumed for the empirically determined nuclear reduction factor f_n, this causes large uncertainties. Within the uncertainty an agreement with the literature values is found for all levels except for the one at $E_x = 2193$ MeV. There are no other experiments apart from that performed by Hicks *et al.* [1, 2] and the one presented here that targeted lifetimes of excited states in the order of femtoseconds for ^{128}Te. It has to be mentioned that an INS-DSAM analysis cannot fully exclude feeding of the observed states from higher-energetic levels that would artificially elongate the measured lifetime. In Ref. [2], different neutron beam energies of $E_n = 2.2$ MeV, 2.8 MeV and 3.3 MeV were employed to reduce this effect at least for levels with excitation energies close to the beam energy. In the particle-γ DSA technique presented here feeding is excluded by the application of excitation-energy gates.

B. Level lifetimes in ^{130}Te

All γ-decays of excited states visible in the spectra that yielded enough statistics to be analyzed with the DSA technique were examined, increasing the lifetime information on low-spin levels in ^{130}Te significantly. In total, lifetimes and upper limits for 18 levels in ^{130}Te could be extracted. 15 of these were determined for the first time. The results are listed in Tab. II.

In most cases, only the strongest γ-transition from these levels could be analyzed. Usually, the limit was set by the statistics. In addition, in some cases the transition energy was below the well-calibrated energy range set by the ^{56}Co calibration measured in parallel. Its emitted γ-ray energies start at 846.770(2) keV [30]. This was, *e.g.*, the case for the strongest transition of the 4^+ state [4] at $E_x = 1982$ keV with a transition energy of $E_\gamma = 349$ keV. Since γ-decays with low energies will only show small shifts as the Doppler-shift scales with the γ-ray energy, γ-decay branches of larger γ-ray energies are favored.

Although for DSAM the analysis of a single γ-decay branch is sufficient to determine the level lifetime, for four levels more than one transition could be used to extract the lifetime. In these cases, the extracted lifetimes are given in Tab. II for each transition branch individually. In all cases, the experimental attenuation factors $F_{exp}(\tau)$ and, therefore, the lifetimes determined from both γ-decay branches agree within their uncertainties. For the level at 2745 keV, the shifts for the γ-decay branch with energy $E_\gamma = 859$ keV deviated from a linear pattern for forward angles. Here, only centroids in detector groups containing backward angles were considered, increasing the uncertainty of the determined attenuation factor and thus the lifetime. Nonetheless, the lifetimes determined from both γ-decay branches are still in agreement.

For some levels, the γ-decay transition exhibited a strong shift with an attenuation factor close to unity and an uncertainty exceeding unity. Those are levels with lifetimes in the range of a few femtoseconds down to subfemtoseconds, thus surpassing the accessible range of the DSA method as applied here. Therefore, for the levels at

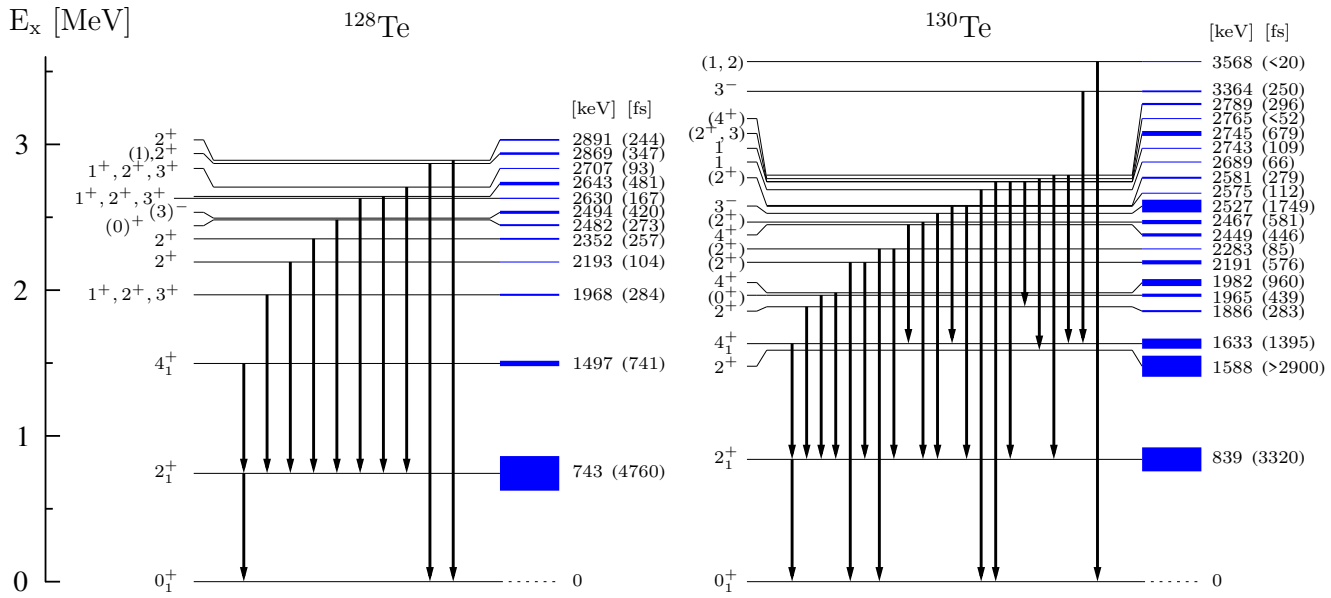

FIG. 6. Level schemes of ^{128}Te and ^{130}Te containing all transitions where lifetimes could be analyzed in this work and decays of the 2_1^+ and 4_1^+ states. For ^{130}Te, the level and lifetime of the 2^+ state at 1588 keV is given as well. The lifetime of each level is indicated by the thickness of the bar next to the level energy (given in keV) as well as given as a separate column in brackets. Here, thicker bars correspond to longer lifetimes. The lifetimes of the 2_1^+ states in ^{128}Te and ^{130}Te are taken from Refs. [3] and [4], respectively. The lifetime of the 2^+ state at 1588 keV in ^{130}Te is taken from Ref. [1].

2765 keV and 3568 keV, only upper limits can be given for the lifetime.

All 18 levels are displayed in a level scheme on the right side of Fig. 6, together with the analyzed transitions and resulting lifetimes. Literature values for the lifetimes of the two lowest 2^+ states [1, 4] are shown, too.

In addition to the 16 lifetimes and two upper limits obtained from the 18 experimental attenuation factors, two definite lower limits could be determined. Lower limits can be assigned when no shift of a transition is observed in the gated spectra, indicating a lifetime longer than detectable with DSAM with the given configuration. In those cases, the de-excitation happens after the recoil nucleus is stopped, which takes about a few picoseconds in the performed experiments, and a lifetime in the order of picoseconds or longer can be assumed. This was observed for the first and second excited 2^+ states at 839 keV and 1588 keV, respectively. For the 5^- state at 2101 keV with a transition energy of 486 keV, no shift was observed as well. However, this transition energy lies below the well-calibrated energy region. Therefore, it cannot be excluded that a possible small shift is concealed by deviating calibrations of the different germanium detectors at small energies. The same holds true for the (4^+) state at 2330 keV with a transition energy of $E_\gamma = 698$ keV, although this transition energy is much closer to the well-calibrated energy region. For both levels, a lower limit is tentatively assumed.

C. ^{130}Te: Comparison with literature values

Already published lifetimes of levels in ^{130}Te stem from an inelastic neutron scattering (INS) DSAM experiment followed by γ-ray spectroscopy performed at the 7 MV electrostatic accelerator lab of the University of Kentucky [1]. It was designed to study the first six excited 2^+ states to investigate the structure of possible mixed-symmetry states. Lifetimes for three of these levels could be remeasured in the present work. For comparison, the lifetimes obtained by Hicks *et al.* [1] are included in Tab. II. The analysis of the lifetimes of the 2_1^+ and 2_2^+ yielded no visible shift in the gated spectra of the angular groups and therefore indicate lifetimes of these states of a few picoseconds or longer. This is in accordance with the lifetimes reported in [1] and [4] which place them above 2.9 ps.

In comparison with the literature values, the remeasured lifetime for the tentative 2^+ state at $E_x = 2191$ keV agrees with the previous values. In the other two cases at $E_x = 1886$ keV and $E_x = 2283$ keV, the newly measured lifetimes are shorter than those given in [1]. Longer lifetimes might be a result of feeding, which cannot be excluded in the neutron scattering experiments as explained above.

The origin of the γ-decay branches used for the determination of the lifetime of these states was studied to resolve whether the discrepancy originated from feeding of the levels studied in the INS-DSAM experiment. For

TABLE II. Lifetimes of levels in ^{130}Te. Experimental attenuation factors $F_{exp}(\tau)$ and lifetimes τ are given. For levels where the lifetime was extracted from two transitions a weighted average of the lifetime τ_{av} is given, obtained from the weighted average of the attenuation factors. Excitation energies E_x of the levels with spin and parity J_i^π as well as the transition energies E_γ to the level with spin and parity J_f^π are taken from [4]. Statistical and systematic uncertainties for the lifetimes, $\Delta\tau_{stat}$ and $\Delta\tau_{sys}$, respectively, are stated as $\tau \pm \Delta\tau_{stat} \pm \Delta\tau_{sys}$. For the attenuation factors, only statistical uncertainties are given. Spins annotated with ? are unknown. τ_{lit} are taken from [1]. From mixing ratios given in [4] and the lifetimes, $B(E2)\downarrow$ and $B(M1)$ transition strengths were calculated. Due to the asymmetric uncertainties of the lifetimes, Gaussian error propagation is not possible. Instead, the boundary values of the lifetimes were used to calculate intervals for the transition strengths, with the width of these intervals given in the way as upper and lower uncertainties are shown. The intervals were calculated for $\Delta\tau_{stat}$ and $\Delta\tau_{sys}$ individually and added quadratically in the respective direction.

E_x [keV]	J_i^π	E_γ [keV]	J_f^π	$F_{exp}(\tau)$	τ [fs]	τ_{av} [fs]	τ_{lit} [fs]	$B(E2)\downarrow$ [e^{2}fm^4] [a]	$B(M1)$ [μ_N^2] [a]
1633	4^+	794	2^+	0.10(2)	$1395^{+342\ +150}_{-237\ -124}$			1859^{+422}_{-408}	
1886	2^+	1046	2^+	0.36(6)	$283^{+93\ +30}_{-65\ -26}$		470^{+40}_{-30}	67^{+25}_{-22}	0.17^{+6}_{-5}
1965	(0^+)	1125	2^+	0.25(8)	$439^{+255\ +46}_{-135\ -42}$			1030^{+470}_{-391} [b]	
1982	4^+	1142	2^+	0.14(2)	$960^{+186\ +99}_{-139\ -89}$			180^{+45}_{-43}	
2191	(2^+)	1351	2^+	0.23(4)	$523^{+145\ +55}_{-100\ -48}$	$576^{+100\ +61}_{-78\ -53}$	590(50)	10(3)	0.018^{+5}_{-4}
		2191	0^+	0.20(3)	$615^{+151\ +65}_{-107\ -67}$			14(4)	
2283	(2^+)	1443	2^+	0.65(5)	$90^{+20\ +9}_{-18\ -8}$	$85^{+15\ +9}_{-13\ -8}$	150(10)	13^{+4}_{-3}	0.18(5)
		2283	0^+	0.68(6)	$79^{+24\ +8}_{-20\ -7}$			27^{+8}_{-7}	
2449	4^+	816	4^+	0.26(3)	$446^{+64\ +48}_{-52\ -40}$			206^{+41}_{-40}	0.22(4)
2467	(2^+)	1627	2^+	0.21(2)	$581^{+76\ +60}_{-63\ -55}$				
2527	3^-	1688	2^+	0.08(4)	$1749^{+2058\ +184}_{-651\ -162}$				
2575	?	942	4^+	0.6(2)	$112^{+132\ +12}_{-68\ -10}$			9812^{+15194}_{-5392} [c]	
2581	(2^+)	1741	2^+	0.35(3)	$279^{+33\ +30}_{-28\ -26}$				
2689	1	2689	0^+	0.72(9)	$66^{+31\ +6}_{-25\ -6}$				
2743	1	2743	0^+	0.6(2)	$109^{+102\ +11}_{-59\ -10}$				
2745	$(2^+,3)$	859	2^+	0.16(4)	$811^{+283\ +83}_{-177\ -74}$	$679^{+61\ +69}_{-53\ -62}$			
		1905	2^+	0.19(1)	$664^{+63\ +68}_{-55\ -60}$				
2765	(4^+)	1177	2^+	0.9(1)	<52			>3059	
2789	?	1156	4^+	0.5(2)	$165^{+159\ +18}_{-79\ -15}$	$296^{+51\ +32}_{-41\ -27}$		267^{+51}_{-47} [c]	
		1950	2^+	0.33(4)	$307^{+55\ +33}_{-44\ -28}$				
3364[d]	3^-	1479	2^+	0.38(1)	$250^{+13\ +28}_{-12\ -22}$				
3568	$(1,2)$	3568	0^+	1.1(2)	<20				

[a] Intervals are given instead of uncertainties. See cation.
[b] Calculated assuming only $E2$ transition as mixing is unknown.
[c] Tentatively calculated for an $E2$ transition since the spin and parity of the initial state are unknown.
[d] Obtained from the γ-ray energies following its de-excitation (see Sec. IV D).

this, a narrow gate on the respective transition energy was applied each time, yielding a spectrum containing all coincident protons responsible for an excitation with following γ-decay of the gated energy, calibrated for the corresponding excitation energy. A possible feeding in (n,n'γ) is discussed in the following for the three lifetimes that can be compared with results from Ref. [1].

The 2^+ level at 1886 keV: A section of the spectrum gained by gating on the strongest transition of the 2_3^+ state at $E_x = 1886$ keV with $E_\gamma = 1046$ keV is given in the upper part of Fig. 7. The excitation of the level of interest at 1886 keV is clearly visible, as well as the excitation of the $(2^+,3)$ level at 2745 keV, which decays into the 1886 keV level [4]. Further excitations of levels with subsequent γ-decays of $E_\gamma = 1046$ keV are visible around 3360 keV and 3150 keV. Red lines indicate the two beam energies applied in the INS-DSAM experiment of $E_n = 2.2$ MeV and $E_n = 3.4$ MeV. For the determination of the 2_3^+ lifetime, the lower beam energy was used to reduce possible feeding [1]. In the excitation spectrum in Fig. 7 no excitations with a transition energy of $E_\gamma = 1046$ keV other than that of the level of interest itself are visible below this energy. Assuming a similar excitation mechanism for both (p,p'γ) and (n,n'γ) this excludes feeding as the cause for the discrepancy.

The 2^+ level at 2191 keV: Since the neutron-beam energy was chosen directly above the excitation of the level at 2191 keV feeding can also be excluded for this state. This is supported by the lifetimes obtained from the two analyzed γ-decay branches of this level in the present analysis. Both lifetimes agree with each other as well as with the one measured by [1], confirming the

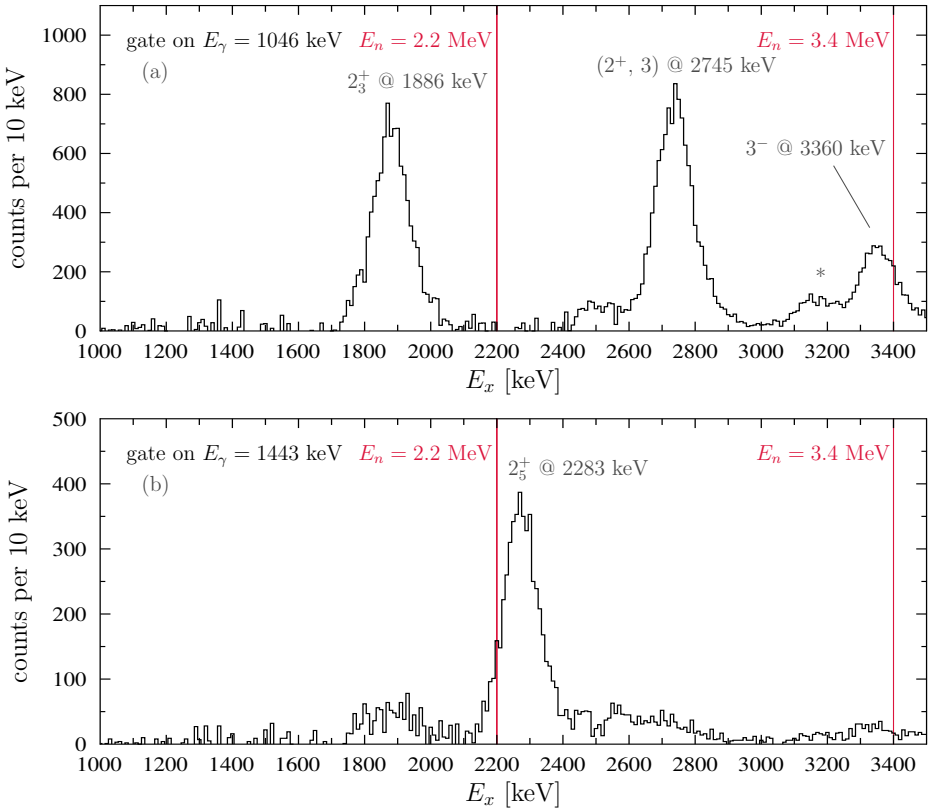

FIG. 7. Excitation-energy spectra obtained by gating on the transitions with (a) $E_\gamma = 1046$ keV and (b) $E_\gamma = 1443$ keV in ^{130}Te. Known levels are indicated by their spin and parity as well as level energy. The neutron beam energies employed in [1] are marked by vertical lines.

known lifetime.

The 2^+ level at 2283 keV: The possible 2^+ state at $E_x = 2283$ keV lies above the employed lower neutron-beam energy and was therefore deduced from the INS-DSAM experiment using $E_n = 3.4$ MeV. Although the energy gap between the beam energy and the excitation energy of the level of interest is larger than 1 MeV and poses the possibility of feeding levels in between, no other excited levels in this energy region de-exiting via a similar energy are known in the level scheme [4]. When gating on the strongest transition with $E_\gamma = 1443$ keV, as shown in the lower panel of Fig. 7, a shallow but broad peak between 2600 keV and 2800 keV, however, indicates the existence of some levels with following γ-decays of energies similar to 1443 keV. A gate on the levels at 2745 keV and 2765 keV reveals subsequent transitions with γ-energies of 460 keV and 482 keV, respectively. These energies correspond to the difference to the level energy 2283 keV and can thus likely be placed in the level scheme, indicating that a feeding of this state does indeed exist below the applied neutron-beam energy. For both levels, a lifetime could be determined in the present analysis. Although the lifetime of the level at 2765 keV is very short and only an upper limit of 52 fs can be given, the state at 2745 keV has a much longer lifetime of around 700 fs. As a feeder, this would lengthen the determined lifetime for the state at 2283 keV and might explain the difference in the compared lifetimes.

Another small enhancement in the spectrum just below $E_n = 3.4$ MeV is observed around 3360 keV. In [4], a level at 3360(10) keV is proposed with no known transitions. An excitation-energy gate on that energy reveals several transitions that fit in the level scheme, amongst them a transition with $E_\gamma = 1081$ keV that leads to the level at 2283 keV. This introduces another possible, although very weak feeder. Its lifetime was determined to be $250^{+13}_{-12}\ ^{+28}_{-22}$ fs in this work. The lifetime of the 2_5^+ state at 2283 keV was determined separately from two γ-decay branches in this work. Both transitions yield lifetimes that are in excellent agreement with each other, validating the newly determined lifetime. Therefore, a new lifetime as given in Tab. II is proposed for this level.

D. Extension of the ^{130}Te level scheme

Using excitation- and transition-energy gates, several new transitions could be added to the level scheme of

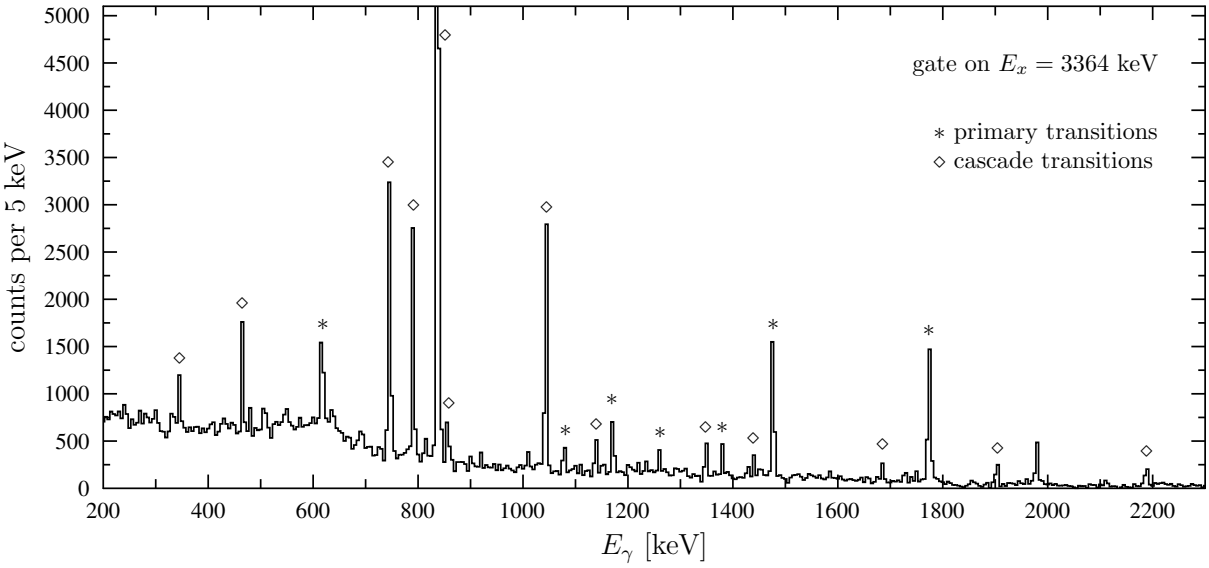

FIG. 8. γ-decay spectrum after gating on the excitation energy of the 3^- level at $E_x = 3364$ keV. All γ-decays identified as primary transitions are marked by an asterisk. Subsequent γ-decays are marked with a diamond.

TABLE III. Hitherto unknown transitions from excited states of ^{130}Te observed in the (p,p'γ) data. Spins and parities for the initial and final states J_i^π and J_f^π as well as the level energy of the final states E_f are taken from [4] if not stated otherwise, as well as the excitation energies E_x of the levels at 2745 keV and 2765 keV. All other level energies are calculated from the transition energies E_γ and the final level energies. The transition energies and their uncertainties were determined by fitting the peak in the excitation-energy gated spectrum obtained from the pγ-coincidence matrix and considering an uncertainty in the energy calibration depending on the transition energy.

E_x [keV]	J_i^π	E_γ [keV]	E_f [keV]	J_f^π
2744.97(4)	$(2^+,3)$	309.1(5)	2435.59(4)	4^-
		462.0(5)	2282.593(25)	(2^+)
		553.6(5)	2190.615(23)	(2^+)
2765.26(22)	(4^+)	481.6(5)	2282.593(25)	(2^+)
3177.0(20)	$(3^-,4^+)^a$	1075.3(2)	2101.25(3)	5^-
		1290.6(1)	1885.700(25)	2^+
3193.7(4)	$(1,2^+)^a$	3193.7(4)	0.0	0^+
3364.1(5)	3^-	619.2(1)	2744.97(4)	$(2^+,3)$
		1081.0(3)	2282.593(25)	(2^+)
		1173.5(1)	2190.615(23)	(2^+)
		1262.3(2)	2101.25(3)	5^-
		1382.6(2)	1981.546(23)	4^+
		1478.4(1)	1885.700(25)	2^+
		1776.2(1)	1588.256(24)	2^+

[a]Tentatively assigned

^{130}Te, as listed in Tab. III.

As mentioned above, a 3^- state at 3360(10) keV [4] was observed when searching for possible feeding of the 2^+ state at 1886 keV, as shown in the upper panel of Fig. 7. An excitation-energy gate on the region with the proposed level energy revealed seven new transitions that can be placed in the level scheme, with subsequent γ-decays which all together provide a consistent picture of the level scheme. The resulting gated γ-ray spectrum is shown in Fig. 8. For better visibility of the peaks, the spectrum was rebinned to 5 keV per bin. All new transition energies and the energies of the resulting final states are given in Tab. III. From those, the level energy and its uncertainty could be calculated. As mentioned above, the level lifetime was determined as well.

The newly observed transitions for the levels at 2745 keV and 2765 keV that were discussed in the previous section are also given in Tab. III. Two additional transitions of the 2745 keV level are also listed. Since in all four cases the transition energy lies below the calibration-sensitive region, a systematic uncertainty of 0.5 keV was estimated.

Another level with formerly unknown γ-decays and an uncertainty in excitation energy of 20 keV was observed in the feeding analysis. Located in Ref. [4] at 3180 keV, its energy could be restrained to 3177(2) keV by the observation of two γ-decays with $E_\gamma = 1075.3(2)$ keV and 1290.6(1) keV. It was observed as a possible feeder for the 1886 keV level and is indicated in the upper panel of Fig. 7 by an asterisk. This is supported by the observed decay energy of 1290.6(1) keV which corresponds to the energy difference between both levels. Although the level was too weakly excited to determine a lifetime by the DSA method, it was possible to tentatively assign spins and parities of $(3^-,4^+)$ from the final states when assuming predominantly E1, E2 and M1 transitions.

Finally, a new ground-state transition was observed

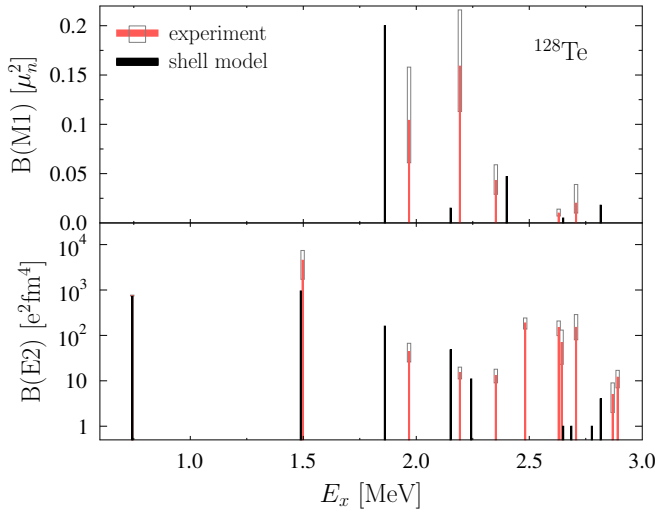

FIG. 9. $B(M1)$ and $B(E2)$ transition strengths in ^{128}Te. The experimental transition strengths calculated from the lifetimes determined in this work as given in Tab. I are shown in red with gray boxes illustrating the uncertainty. In black (without boxes), transition-strength results from a shell-model calculation are given. For more details on the shell-model calculation, see text.

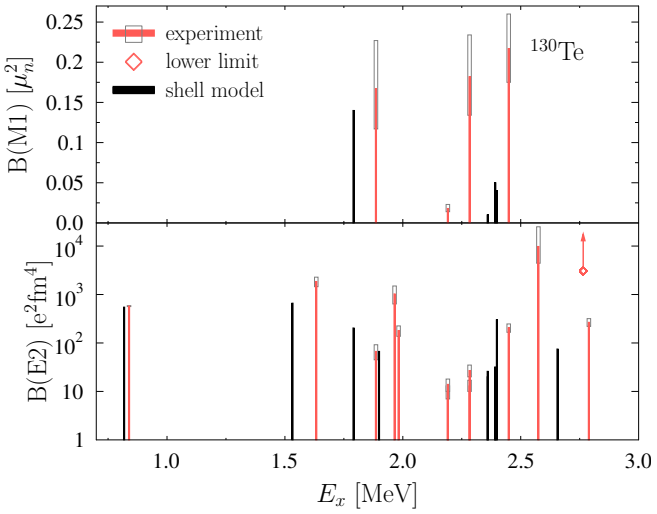

FIG. 10. Same as Fig. 9 but for ^{130}Te. For levels where transition strengths were determined for more than one decay transition, both are shown. At 2765 keV, the lower limit is indicated by a diamond with arrow.

of a formerly unknown level at $E_x = 3194$ keV. Again, the level was too weakly excited to deduce a lifetime by dividing the data into several angular groups. A tentative spin and parity was assigned under the same assumptions as above.

E. Shell-model calculations

To compare the new experimental findings to theoretical predictions, shell-model calculations were performed using the code NuShellX [31] in the $jj55pn$ model space above a ^{100}Sn core, consisting of the $0g_{7/2}, 1d_{5/2}, 1d_{3/2}, 2s_{1/2}, 0h_{11/2}$ orbitals for proton particles and neutron holes. Single-particle energies are taken from excited states in ^{133}Sb [32] and ^{131}Sn [33] for protons and neutrons, respectively, where the proton $2s_{1/2}$ level was estimated at -7.34 MeV [34]. A realistic interaction based on a G matrix derived from a CD-Bonn nucleon-nucleon potential is used, details can be found in Ref. [34]. The Hamiltonian is composed of four terms that describe the neutron-neutron, proton-neutron, proton-proton and Coulomb repulsion between protons separately. Reduced $E2$ transition probabilities were calculated using the effective charges $(e_\pi, e_\nu) = (1.7e, 0.8e)$ as in previous studies [35] to reproduce experimental $B(E2)$ values in the semi-magic ^{134}Te and ^{128}Sn nuclei. $B(M1)$ strengths were calculated with a g factor quenching of 0.7 with respect to g_{free}.

The $B(E2)$ and $B(M1)$ values resulting from this calculation are shown in Fig. 9 for ^{128}Te and in Fig. 10 for ^{130}Te as simple bars. All values experimentally obtained in this work as well as the $B(E2)$ value for the first excited state are given as bars with boxes that indicate the uncertainties. The derived experimental $B(E2)$ values correspond to, *e.g.*, $1.1^{+0.7}_{-0.4}$ W.u. for the $E_\gamma = 1225$ keV transition from the level at $E_x = 1968$ keV in ^{128}Te.

Within the calculation, not all experimental levels could be identified due to lack of spectroscopic data. Although for some levels the theoretically predicted and experimentally determined excitation energies agree within less than 50 keV, the deviations for higher-energetic levels become larger. In both nuclei, the experimental transition strengths for the first excited 2_1^+ states calculated from the lifetimes in the literature [3, 4] match the results of the calculation.

Additionally, the shell-model results include transition strengths for levels that could not be analyzed experimentally. These are shown in Figs. 9 and 10 as well.

In general, the shell-model calculations partly agree with the experimental results, as visible when comparing neighboring bars in Figs. 9 and 10. For ^{128}Te, most of the theoretical $B(M1)$ values are consistent with the experiment, whereas the calculations tend to overestimate the $B(E2)$ transitions strengths for low-lying levels, while reproducing the overall trend and even underestimating them for higher-lying states. In the region between 2.6 MeV and 2.8 MeV, the shell model predicts rather low upper limits for the $B(E2)$ values of 1 e^{2}fm^4, clearly underestimating the experimental findings. In the case of ^{130}Te, the difference in excitation energy of states that can be matched by spin is larger than in the case of ^{128}Te. Thus, states comparable in spin and parity are not necessarily neighboring in Fig. 10. For the four $B(M1)$ transition strengths determined by the shell-model cal-

TABLE IV. Dominant shell-model configurations of excited 2^+ states in ^{128,130}Te as calculated in this work. Only the strongest two components of the wave function are given with the percentage of their contribution. Furthermore, the theoretical excitation energy is also given.

Nucleus	J^π	E_x [MeV]	Configuration	[%]
^{128}Te	2_1^+	0.744	$\pi(0g_{7/2}^2)\nu(1d_{3/2}^{-2}0h_{11/2}^{-4})$	14.3
			$\pi(0g_{7/2}^2)\nu(1d_{3/2}^{-2}2s_{1/2}^{-2}0h_{11/2}^{-2})$	8.5
	2_2^+	1.469	$\pi(0g_{7/2}^2)\nu(1d_{3/2}^{-2}0h_{11/2}^{-4})$	13.2
			$\pi(0g_{7/2}^2)\nu(1d_{3/2}^{-2}2s_{1/2}^{-2}0h_{11/2}^{-2})$	11.9
	2_3^+	1.861	$\pi(0g_{7/2}^2)\nu(1d_{3/2}^{-2}0h_{11/2}^{-4})$	13.5
			$\pi(0g_{7/2}^2)\nu(1d_{3/2}^{-1}2s_{1/2}^{-1}0h_{11/2}^{-4})$	7.0
	2_4^+	2.152	$\pi(0g_{7/2}^2)\nu(1d_{3/2}^{-2}0h_{11/2}^{-4})$	7.0
			$\pi(0g_{7/2}^2)\nu(1d_{3/2}^{-3}2s_{1/2}^{-1}0h_{11/2}^{-2})$	4.5
	2_5^+	2.400	$\pi(0g_{7/2}^1d_{5/2}^1)\nu(1d_{3/2}^{-2}0h_{11/2}^{-4})$	10.8
			$\pi(0g_{7/2}^2)\nu(1d_{3/2}^{-2}0h_{11/2}^{-4})$	7.9
	2_6^+	2.491	$\pi(0g_{7/2}^2)\nu(1d_{3/2}^{-2}0h_{11/2}^{-4})$	6.9
			$\pi(0g_{7/2}^2)\nu(1d_{3/2}^{-2}2s_{1/2}^{-2}0h_{11/2}^{-2})$	5.2
	2_7^+	2.650	$\pi(0g_{7/2}^2)\nu(1d_{3/2}^{-2}0h_{11/2}^{-4})$	14.0
			$\pi(0g_{7/2}^2)\nu(1d_{3/2}^{-2}2s_{1/2}^{-2}0h_{11/2}^{-2})$	13.0
	2_8^+	2.686	$\pi(0g_{7/2}^2)\nu(1d_{3/2}^{-2}0h_{11/2}^{-4})$	11.8
			$\pi(0g_{7/2}^2)\nu(1d_{3/2}^{-3}2s_{1/2}^{-1}0h_{11/2}^{-2})$	11.5
	2_9^+	2.777	$\pi(0g_{7/2}^2)\nu(1d_{3/2}^{-2}0h_{11/2}^{-4})$	8.5
			$\pi(0g_{7/2}^1d_{5/2}^1)\nu(1d_{3/2}^{-2}0h_{11/2}^{-4})$	4.0
^{130}Te	2_1^+	0.818	$\pi(0g_{7/2}^2)\nu(1d_{3/2}^{-2}0h_{11/2}^{-4})$	27.7
			$\pi(0g_{7/2}^2)\nu(1d_{3/2}^{-1}2s_{1/2}^{-1}0h_{11/2}^{-4})$	11.3
	2_2^+	1.522	$\pi(0g_{7/2})\nu(1d_{3/2}^{-2}0h_{11/2}^{-4})$	33.9
			$\pi(0g_{7/2}^2)\nu(1d_{3/2}^{-1}2s_{1/2}^{-1}0h_{11/2}^{-4})$	8.7
	2_3^+	1.791	$\pi(0g_{7/2}^2)\nu(1d_{3/2}^{-1}2s_{1/2}^{-1}0h_{11/2}^{-4})$	20.4
			$\pi(0g_{7/2})\nu(1d_{3/2}^{-2}0h_{11/2}^{-4})$	20.3
	2_4^+	2.360	$\pi(0g_{7/2}^1d_{5/2}^1)\nu(1d_{3/2}^{-2}0h_{11/2}^{-4})$	15.2
			$\pi(0g_{7/2}^2)\nu(1d_{3/2}^{-2}0h_{11/2}^{-4})$	4.5
	2_5^+	2.392	$\pi(0g_{7/2}^2)\nu(1d_{3/2}^{-2}0h_{11/2}^{-4})$	29.5
			$\pi(0g_{7/2}^2)\nu(1d_{3/2}^{-2}2s_{1/2}^{-2}0h_{11/2}^{-2})$	8.2
	2_6^+	2.491	$\pi(0g_{7/2}^2)\nu(1d_{3/2}^{-2}0h_{11/2}^{-4})$	19.4
			$\pi(0g_{7/2}^2)\nu(1d_{3/2}^{-3}2s_{1/2}^{-1}0h_{11/2}^{-2})$	13.0
	2_7^+	2.656	$\pi(0g_{7/2}^1d_{5/2}^1)\nu(1d_{3/2}^{-2}0h_{11/2}^{-4})$	7.9
			$\pi(0g_{7/2}^2)\nu(1d_{3/2}^{-1}2s_{1/2}^{-1}0h_{11/2}^{-4})$	7.8
	2_8^+	2.82	$\pi(0g_{7/2})\nu(1d_{3/2}^{-2}0h_{11/2}^{-4})$	15.0
			$\pi(0g_{7/2}^2)\nu(1d_{3/2}^{-1}2s_{1/2}^{-1}0h_{11/2}^{-4})$	12.0
	2_9^+	2.962	$\pi(0g_{7/2}^2)\nu(1d_{3/2}^{-2}0h_{11/2}^{-4})$	16.4
			$\pi(0g_{7/2}^2)\nu(1d_{3/2}^{-1}2s_{1/2}^{-1}0h_{11/2}^{-4})$	7.7
	2_{10}^+	3.006	$\pi(0g_{7/2}^2)\nu(1d_{3/2}^{-2}0h_{11/2}^{-4})$	16.3
			$\pi(0g_{7/2}^2)\nu(1d_{3/2}^{-2}2s_{1/2}^{-2}0h_{11/2}^{-2})$	12.9

culation, half are in agreement with the measurement, whereas the other half is underestimated by the calculation. Although the calculated $B(E2)$ values do not agree with the experimental ones within their uncertainty, for the majority of levels that could be matched via spin and parity, the correct order of magnitude is reproduced as well as the overall trend. Nevertheless, due to the large differences in excitation energy, only tentative assignments are possible.

The configurations of excited 2^+ states in ^{128,130}Te are given in Tab. IV. As one would expect, the states are more fragmented in ^{128}Te compared to ^{130}Te which can be seen by the smaller amplitudes in ^{128}Te. Independently of the nucleus, the main proton contribution comes from both valence protons in the lowest-lying $\pi(0g_{7/2})$ orbital. For the neutrons, the strongest component arises from the $\nu(1d_{3/2}^{-2}0h_{11/2}^{-4})$ configuration. Furthermore, a competition between excitations in the $1d_{3/2}$ and $2s_{1/2}$ is present for most of the 2^+ states.

V. CONCLUSION

In this work, nuclear level lifetimes for 29 states in ^{128,130}Te could be determined via the pγ-coincidence DSA technique. Comparisons with existing lifetime values showed good agreement. In the case of the 2^+ level at 2283 keV in ^{130}Te, the existing lifetime value could be improved through the analysis and elimination of feeding, made possible by the use of pγ coincidences. These coincidences also allowed the extension of the level scheme of ^{130}Te, as transitions can be easily attributed to levels by the application of excitation-energy gates. In total, 14 new transitions and one new level were identified and two level energies were determined to a higher precision.

Shell-model calculations were performed for ^{128}Te and ^{130}Te which yielded $B(E2)$ and $B(M1)$ transition strengths. These were only partially in agreement with the experimental results, although an overall trend was reproduced. The level energies calculated for ^{130}Te showed a larger deviation from the experimental values as those for ^{128}Te, which were in good agreement.

The observation of large $B(M1)$ values in the order of 0.1-0.2 μ_n^2 in both nuclei supports the interpretation of the corresponding states as mixed-symmetry states. This is partly supported by the shell-model calculation and further spectroscopic data is needed to allow for a better comparison of transition probabilities.

ACKNOWLEDGMENTS

The authors thank A. Blazhev and K.-O. Zell of the IKP Cologne for the production of the targets as well as the accelerator staff for their help with the experiments. We also thank H.-W. Becker for his support during the RBS measurement and P. Petkov for his work on the Monte-Carlo simulation code. This work was supported by the Deutsche Forschungsgemeinschaft under contract No. ZI 510/9-1.

[1] S. F. Hicks, J. R. Vanhoy, and S. W. Yates, Phys. Rev. C **78**, 054320 (2008).
[2] S. F. Hicks, J. C. Boehringer, N. Boukharouba, C. Fransen, S. R. Lesher, J. M. Mueller, J. R. Vanhoy, and S. W. Yates, Phys. Rev. C **86**, 054308 (2012).
[3] Z. Elekes and J. Timar, Nucl. Data Sheets **129**, 191 (2015).
[4] B. Singh, Nucl. Data Sheets **93**, 33 (2001).
[5] N. Pietralla, P. von Brentano, and A. F. Lisetskiy, Prog. Part. Nucl. Phys. **60**, 225 (2008).
[6] P. J. Nolan and J. F. Sharpey-Schafer, Rep. Prog. Phys. **42**, 1 (1979).
[7] R. G. Stokstad, I. A. Fraser, J. S. Greenberg, S. H. Sie, and D. A. Bromley, Nuclear Physics A **156**, 145 (1970).
[8] T. K. Alexander and J. S. Forster, Adv. Nucl. Phys. **10**, 197 (1978).
[9] T. Belgya, G. Molnár, and S. W. Yates, Nucl. Phys. A **607**, 43 (1996).
[10] P. Petkov, D. Tonev, J. Gableske, A. Dewald, and P. von Brentano, Nucl. Instr. and Meth. A **437**, 274 (1999).
[11] A. Hennig, V. Derya, M. N. Mineva, P. Petkov, S. G. Pickstone, M. Spieker, and A. Zilges, Nucl. Instr. and Meth. A **794**, 171 (2015).
[12] S. F. Hicks, J. R. Vanhoy, P. G. Burkett, B. R. Champine, S. J. Etzkorn, P. E. Garrett, S. W. Yates, and M. Yeh, Phys. Rev. C **95**, 034322 (2017).
[13] J. R. Vanhoy, J. A. Tanyi, K. A. Crandell, T. H. Churchill, S. F. Hicks, M. C. Burns, P. A. Roddy, N. V. Warr, T. B. Brown, and S. R. Lesher, Phys. Rev. C **69**, 064323 (2004).
[14] S. G. Pickstone, M. Weinert, M. Färber, F. Heim, E. Hoemann, J. Mayer, M. Müscher, S. Prill, P. Scholz, M. Spieker, V. Vielmetter, J. Wilhelmy, and A. Zilges, Nucl. Instr. and Meth. A **875**, 104 (2017).
[15] F. Heim, J. Mayer, M. Müller, P. Scholz, M. Weinert, and A. Zilges, Nucl. Instr. and Meth. A **966**, 163854 (2020).
[16] L. Netterdon, V. Derya, J. Endres, C. Fransen, A. Hennig, J. Mayer, C. Müller-Gatermann, A. Sauerwein, P. Scholz, M. Spieker, and A. Zilges, Nucl. Instr. and Meth. A **754**, 94 (2014).
[17] W.-K. Chu, J. Mayer, and M.-A. Nicolet, *Backscattering spectrometry* (Academic Press, Inc., 1978).
[18] M. Mayer, AIP Conference Proceedings **475**, 541 (1999).
[19] J. Lindhard, M. Scharff, and H. E. Schiøtt, Mat. Fys. Medd. Dan. Vid. Selak. **33**, 1 (1963).
[20] J. Lindhard, V. Nielsen, and M. Scharff, Mat. Fys. Medd. Dan. Vid. Selak. **36** (1968).
[21] W. M. Currie, Nucl. Instr. and Meth. **73**, 173 (1969).
[22] P. Petkov, J. Gableske, O. Vogel, A. Dewald, P. von Brentano, R. Krücken, R. Peusquens, N. Nicolay, A. Gizon, J. Gizon, D. Bazzacco, C. Rossi-Alvarez, S. Lunardi, P. Pavan, D. R. Napoli, W. Andrejtscheff, and R. V. Jolos, Nucl. Phys. A **640**, 293 (1998).
[23] J. Keinonen, AIP Conference Proceedings **125**, 557 (1985).
[24] L. C. Northcliffe and R. F. Schilling, Nuclear Data Tables **A7**, 233 (1970).
[25] J. F. Ziegler and J. P. Biersack, *Treatise on Heavy-Ion Science: Volume 6: Astrophysics, Chemistry, and Condensed Matter, Chapter: The Stopping and Range of Ions in Matter* (Springer US, Boston, MA, 1985).
[26] J. F. Ziegler and W. K. Chu, At. Data Nucl. Data Tables **13**, 463 (1974).
[27] G. Winter, Nucl. Instr. and Meth. **214**, 537 (1983).
[28] G. Winter, Technical report ZfK-497, ZfK Rossendorf (1983).
[29] E. E. Peters, A. Chakraborty, B. P. Crider, B. H. Davis, M. K. Gnanamani, M. T. McEllistrem, F. M. Prados-Estévez, J. R. Vanhoy, and S. W. Yates, Phys. Rev. C **88**, 024317 (2013).
[30] H. Junde, H. Su, and Y. Dong, Nucl. Data Sheets **112**, 1513 (2011).
[31] B. A. Brown and W. D. M. Rae, Nucl. Data Sheets **120**, 115 (2014).
[32] Y. Khazov, A. Rodionov, and F. G. Kondev, Nucl. Data Sheets **112**, 855 (2011).
[33] Y. Khazov, I. Mitropolsky, and A. Rodionov, Nucl. Data Sheets **107**, 2715 (2006).
[34] B. A. Brown and W. D. M. Rae, Phys. Rev. C **71**, 044317 (205).
[35] T. J. Gray, J. M. Allmond, A. E. Stuchbery, C.-H. Yu, C. Baktash, A. Gargano, A. Galindo-Uribarri, D. C. Radford, J. C. Batchelder, J. R. Beene, C. R. Bingham, L. Coraggio, A. Covello, M. Danchev, C. J. Gross, P. A. Hausladen, N. Itaco, W. Krolas, J. F. Liang, E. Padilla-Rodal, J. Pavan, D. W. Stracener, and R. L. Varner, Phys. Rev. Lett. **124**, 032502 (2020).